

# Increasing the Fisher Information Content through Moving-Mesh Reconstruction

Qiaoyin Pan,<sup>1,2,\*</sup> Ue-Li Pen,<sup>2,3,4,5,†</sup> Derek Inman,<sup>2,6</sup> and Hao-Ran Yu<sup>2,7</sup>

<sup>1</sup>*School of Physics, Nankai University, 94 Weijin Rd, Nankai, Tianjin, 300071, China*

<sup>2</sup>*Canadian Institute for Theoretical Astrophysics, University of Toronto,  
60 St. George Street, Toronto, Ontario M5S 3H8, Canada*

<sup>3</sup>*Dunlap Institute for Astronomy and Astrophysics,  
University of Toronto, Toronto, ON M5S 3H4, Canada*

<sup>4</sup>*Canadian Institute for Advanced Research, Program in Cosmology and Gravitation*

<sup>5</sup>*Perimeter Institute for Theoretical Physics, Waterloo, ON, N2L 2Y5, Canada*

<sup>6</sup>*Department of Physics, University of Toronto, 60 St. George, Toronto, ON M5S 1A7, Canada*

<sup>7</sup>*Kavli Institute for Astronomy and Astrophysics, Peking University, Beijing 100871, China*

(Dated: December 2, 2016)

Reconstruction techniques are commonly used in cosmology to reduce complicated nonlinear behaviour to a more tractable linearized system. We study the *Moving-Mesh* algorithm which is expected to perform better than many alternatives as it is based in Lagrangian space. To quantify the algorithm's ability to reconstruct linear modes, we study the Fisher information presented in 136  $N$ -body simulations before and after reconstruction. We find that the linear scale is pushed to  $k \simeq 0.3 h/\text{Mpc}$  after reconstruction. We furthermore find that the translinear plateau of the cumulative Fisher information is increased by a factor of  $\sim 40$  after reconstruction, from  $I \simeq 2.5 \times 10^{-5}/(\text{Mpc}^3/h^3)$  to  $I \simeq 10^{-3}/(\text{Mpc}^3/h^3)$  at  $k \simeq 1 h/\text{Mpc}$ . This includes the decorrelation between initial and final fields, which has been neglected in many previous studies, and we find that the log-normal transform in this metric only gains a factor of 4 in information. We expect this technique to be beneficial to problems such as baryonic acoustic oscillations and cosmic neutrinos that rely on an accurate disentangling of nonlinear evolution from underlying linear effects.

PACS numbers:

## I. INTRODUCTION

The power spectrum is widely used in modern cosmology to measure the matter fluctuations. In the early universe, initial Gaussian density fields can be completely described by the power spectrum, or the two-point statistics. However, gravitational instability and nonlinear large scale structure (LSS) formation make the matter distribution highly non-Gaussian, and the galaxy distribution also follows this non-Gaussian distribution. In these cases one needs to compute higher statistics which are computationally more expensive and more difficult to interpret into initial cosmological parameters. Fisher information is usually used to quantify the amount of independent information that is contained in the power spectrum estimation.

Rimes and Hamilton [1] first study the Fisher information contained in the matter power spectrum given by  $N$ -body simulations, and find that there is a plateau on translinear scales ( $k \simeq 0.2 - 0.8 h/\text{Mpc}$ ), which shows that on these scales, there is a strong coupling of Fourier modes. Thus the power spectrum on smaller scales, gives little additional independent information.

There are many approaches to recover the lost information in the power spectrum of the matter density field, by transforming the final density field into a more Gaussian, early stage density field. For example, Gaussianization transforms are commonly used [2, 3] to make the loga-

rithmic distribution more Gaussian. Nonlinear Wiener filters are used in wavelet space to Gaussianize the fields and can also improve the Fisher information [4–6]. It is shown in [6] that, although these methods or their combinations may have different abilities to recover the Fisher information, by means of reducing the mode coupling and variances in the auto power spectrum of Gaussianized density fields, they do not necessarily improve the cross correlation between the initial density field and the final density field, and thus result in a smearing out of the baryonic acoustic oscillations (BAO) peak in the two-point correlation function. If one is concerned about mapping the initial conditions to final conditions (e.g. measurement of BAO) these methods are unable to extract valid information from initial conditions, at least in the cross power spectrum between initial and final conditions.

Reconstruction techniques (including the one described in [6]) are able to increase the Fisher information while also improving the cross correlation with the initial conditions and sharpening the BAO peak. It is based on the coupling of linear density field  $\delta_L(\mathbf{q}, t_0)$  to the displacement field  $\Psi(\mathbf{q})$  (first derived by [7]), which is estimated by a smoothed final density field. [8] shows a new method in the estimation of displacement field in 1-dimensional (1D), according to which the 1D linear density field is reconstructed in Lagrangian space and successfully improves the BAO measurement. In 3D cases, it is nontrivial to estimate the displacement field, but [9] shows that the displacement field given by  $N$ -body simulations can be used to recover  $\delta_L$ .

In this paper we generalize the displacement field estimation method from 1D [8] to 3D, reconstruct  $\delta_L$  and

---

\*Electronic address: panda@mail.nankai.edu.cn

†Electronic address: pen@cita.utoronto.ca

study the Fisher information recovery in  $\delta_L$ . Here, the displacement field estimation is done by a *Moving-mesh* (MM) algorithm, which is based on the *Adaptive Particle-mesh* (APM) simulation algorithm [10, 11].

This paper is organized as follows. In Section II, we briefly describe the reconstruction algorithm. In Section III, we present the main steps of the  $N$ -body simulation code that are used to simulate the dark matter density fields, and the result of running the reconstruction code. In Section IV, we calculate and compare the power spectra, correlation matrix and Fisher information given by simulation and reconstruction. The discussion and conclusion are presented in Section V

## II. RECONSTRUCTION ALGORITHM

The aim of the reconstruction is to estimate the Lagrangian position, or the displacement, of particles from their final position only. Due to the highly nonlinear process at the late stage, it is hard to fully describe the displacement field from the final condition. However, since the result in [9] showed that the  $E$ -mode displacement field has a strong correlation with the linear density field on large scale ( $r > 0.5$  when  $k \lesssim 2h/\text{Mpc}$ ), estimating the  $E$ -mode displacement is expected to recover a large amount of information. It can be done by applying *Moving-Mesh* (MM) algorithm described in [12], which is originated from *Adapting Particle-Mesh* (APM) algorithm [10, 11].

The basic idea is to build a Particle-Mesh scheme on a curvilinear coordinate system,  $\xi = (\xi_1, \xi_2, \xi_3)$ , in which number of particles per grid cell is set approximately constant. The displacement of particles in each grid cell is then approximately described by the deformation of the curvilinear grid on the Euclidean coordinate  $\mathbf{x}(\xi, t)$ . Assuming that the deformation is a pure gradient, the physical position of particles on Euler coordinate is given as

$$x^i = \xi^\mu \delta_\mu^i + \Delta x^i, \quad (1)$$

where

$$\Delta x^i = \frac{\partial \phi}{\partial \xi^\nu} \delta^{\nu i}. \quad (2)$$

We use the convention the same as in [10], Latin indices denoting Cartesian coordinate, while Greek indices denoting the curvilinear grid coordinate.  $\phi$  is called the deformation potential, and  $\Delta x^i$  the lattice displacement. The coordinate transformation matrix  $e_\mu^i = \partial x^i / \partial \xi^\mu$  is guaranteed to be positive definite so that the volume element  $\sqrt{g} \equiv \det |e_\mu^i|$  is always positive. This choice of the deformation can minimize the cell-crossing.

To solve the deformation potential  $\phi$ , consider the continuity equation in curvilinear coordinate,

$$\frac{\partial(\sqrt{g}\rho)}{\partial t} + \partial_\mu [\rho \sqrt{g} e_\mu^\nu (v^\nu - \Delta \dot{x}^\nu)] = 0 \quad (3)$$

$\Delta \dot{x}^i = \delta^{\nu i} \partial_\nu \dot{\phi}$  is chosen such that the first term in Eq.3 is zero, resulting in a constant mass per volume element.

The velocity field divergence is replaced by the deviation density field  $\Delta \rho = \bar{\rho} - \rho \sqrt{g}$ , which ideally should be zero. Then the deformation potential is described via the elliptic equation,

$$\partial_\mu (\rho \sqrt{g} e_\mu^\nu \delta^{\nu i} \partial_\nu \Delta \phi) = \Delta \rho. \quad (4)$$

The Eq.4 can be solved using multigrid algorithm described in [10, 11] (see also [12] for brief description). The deformation  $\Delta x^i$  is closer to the displacement of particles when higher resolution is used to describe the density field so that less particles are contained in each grid cell.

## III. IMPLEMENTATION

We use the CUBEP<sup>3</sup>M [13] to run 136 simulations with a box size of  $300 h^{-1} \text{Mpc}$ , affine resolution of  $1024^3$  cells and  $512^3$  totally particles. The initial conditions are computed using the transfer function given by CAMB [14] and then propagating the power linearly back to  $z = 100$  with a growth factor. The Zel'dovich approximation is used to calculate the displacement and velocity fields, which are assigned to the particles. The cosmological parameters used are  $\Omega_M = 0.32$ ,  $\Omega_\Lambda = 0.679$ ,  $h = 0.67$ ,  $\sigma_8 = 0.83$ , and  $n_s = 0.96$ . Different seeds are used to produce the initial conditions for different simulations so that they are independent to each other.

Then we run the MM reconstruction code on the nonlinear density fields from simulation in a resolution of  $ng = 128$  per dimension. The multigrid algorithm is iterated for 1000 times in the result of the root mean square decreasing from  $\sim 4.5$  to  $\sim 0.2$ . A 2D projection of one layer of the deformed grids and the original density field on the grid are given in Fig.1. As expected, there is no grid crossing after reconstruction.

## IV. POWER SPECTRA AND INFORMATION CONTENT

The power spectrum is the Fourier transform of the correlation function and measures the amount of clustering in the matter distribution as a function of wavenumber  $k$ ,

$$\langle \delta(\mathbf{k}) \delta(\mathbf{k}') \rangle = (2\pi)^3 P(\mathbf{k}) \hat{\delta}(\mathbf{k} - \mathbf{k}'), \quad (5)$$

where  $\delta(\mathbf{k})$  is the density fluctuation in wave space, while  $\hat{\delta}$  is the delta function. Of equal interest is  $\Delta^2(k)$ , the power spectrum in its dimensionless form, defined as

$$\Delta^2(k) \equiv \frac{k^3 P(k)}{2\pi^2}. \quad (6)$$

The power spectra of the mass distributions are calculated using the “Nearest Grid Point” (NGP) mass assignment scheme. In Fig.2(a) we plot the mean cross correlation function,  $r = P_{\delta\delta_L} / \sqrt{P_\delta P_{\delta_L}}$  of the nonlinear and the linear power spectrum, and the reconstructed and linear power spectrum respectively. The wave number where the cross correlation drops to a half increases from  $k \simeq$

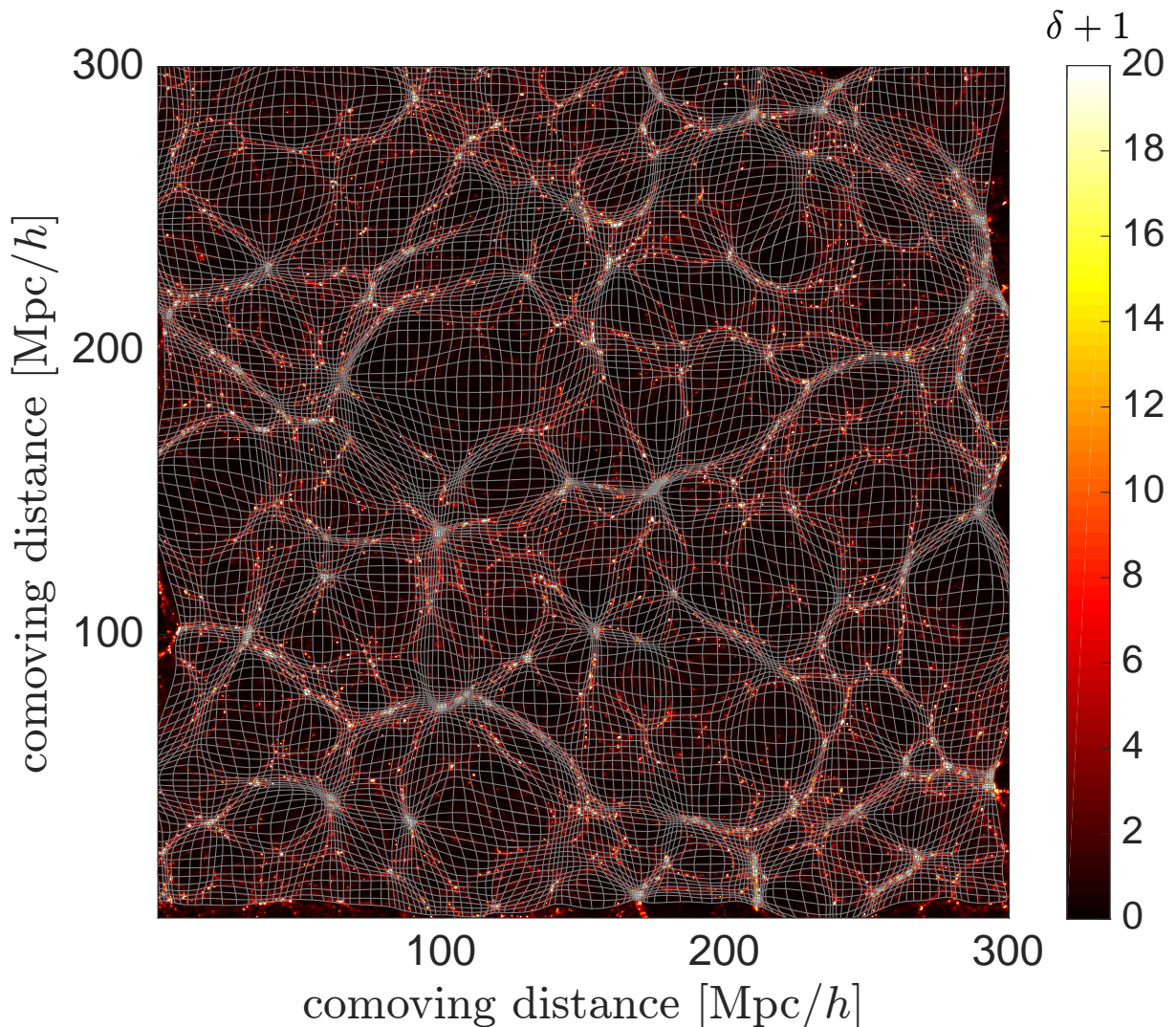


FIG. 1: The 2-D projection of the deformed grid of a sample  $N$ -body simulations is shown as curved white lines. The  $\delta + 1$  field on the deformed grid is shown underneath.

$0.2 h/\text{Mpc}$  to  $k \simeq 0.6 h/\text{Mpc}$  after the reconstruction. To qualify the improvement of cross correlation better, we compute the damping factors  $\mathcal{D}(k) = r^4$  fitting the Gaussian BAO damping models  $\mathcal{D}(k) = \exp(-k^2 \Sigma^2/2)$ . In Fig.2(a) we plot  $\mathcal{D}_\delta^{1/4}$  ( $\Sigma = 11.3 \text{ Mpc}/h$ ) and  $\mathcal{D}_{\delta_R}^{1/4}$  ( $\Sigma = 3.9 \text{ Mpc}/h$ ) over  $r_{\delta_L}$  and  $r_{\delta_R \delta_L}$ . We also plot  $\mathcal{D}(k)^{1/4}$  that match cross correlation function after  $E$ -mode displacement reconstruction in [9] ( $\text{ng} = 512$ , box size =  $400 \text{ Mpc}/h$ ,  $\Sigma = 1.3 \text{ Mpc}/h$ ), and MM reconstruction in a higher resolution in [12] ( $\text{ng} = 512$ , box size =  $600 \text{ Mpc}/h$ ,  $\Sigma = 2.6 \text{ Mpc}/h$ ). We find that in higher resolution, the reconstruction gives a cross correlation damping at smaller scale. And it's expected that the  $E$ -mode displacement reconstruction gives a reconstructed power spectrum more correlated with the initial one, since it completely picks out the irrotational component of the real displacement field in  $N$ -body simulation, while through MM reconstruction, the difference between the reconstructed displacement and the real displacement still contains an irrotational component, which

is also correlated with the linear power spectrum. In Fig.2(b) we plot the linear power spectrum, and mean power spectrum (with error bars) of 136 nonlinear density fields and reconstructed density fields simply given by  $\delta_R = -\nabla^2 \phi$ . The reconstructed power spectrum drops at nonlinear scale ( $k \gtrsim 0.3 h/\text{Mpc}$ ) since the reconstructed density fields are totally irrotational. The result is similar to that of  $E$ -mode displacement reconstruction described in [9], in which the reconstructed power spectrum drops, but in a different scale and at a different speed.

Mathematically, the Fisher information [15]  $I$  in the log of amplitude  $A$  of the initial matter power spectrum is defined as

$$I_A \equiv - \left\langle \frac{\partial^2 \ln \mathcal{L}}{\partial A^2} \right\rangle, \quad (7)$$

in which  $\mathcal{L}$  denotes the likelihood. For Gaussian fluctuations, the likelihood depends on parameters only through the power spectrum  $P(k)$ , so the information  $I$  in  $A$  de-

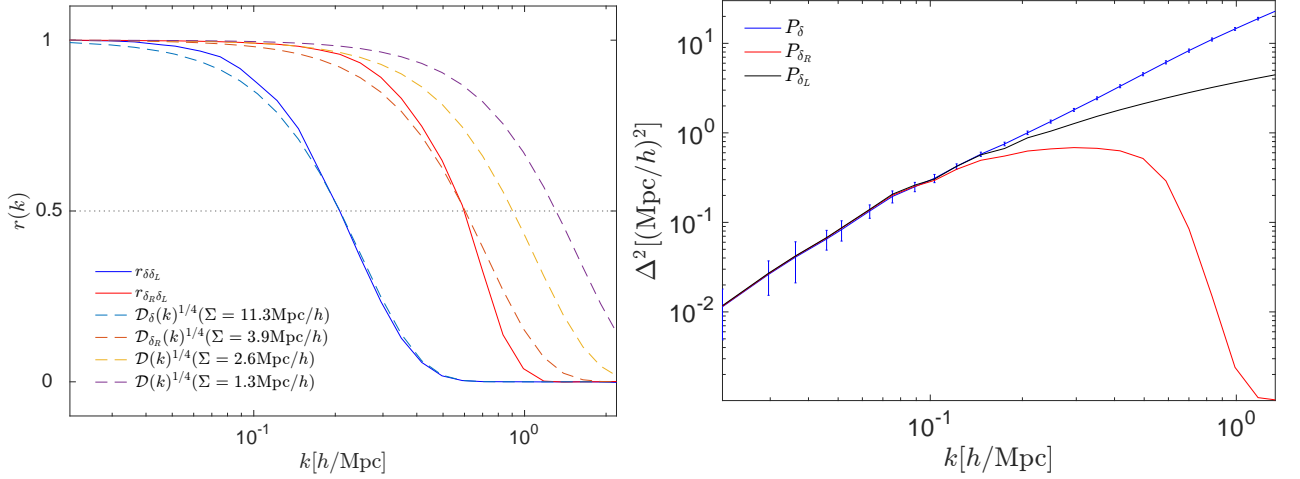


FIG. 2: (a) The cross correlation function (solid lines)  $r_{\delta\delta_L}$  (blue) and  $r_{\delta_R\delta_L}$  (red), and BAO damping models (dash lines). (b) The dimensionless power spectrum computed via linear theory (black), the mean value of 136  $N$ -body simulations with  $1\sigma$  error bars (blue), and reconstruction of the simulations (red).

finied by Eq.7 can be written as [1]

$$I_A = - \left\langle \sum_{k,k'} \frac{\partial \ln P(k)}{\partial \ln A} \frac{\partial^2 \ln \mathcal{L}}{\partial \ln P(k) \partial \ln P(k')} \frac{\partial \ln P(k')}{\partial \ln A} \right\rangle, \quad (8)$$

in which the angle bracket denotes the average over all the power spectra.

The definition Eq.8 can be written in a simpler form in two aspects, one of which is the first and the third partial derivative terms. For any density field  $\delta$ , we can conveniently decompose it into linear and nonlinear components

$$\delta(k) = b(k)\delta_L(k) + n(k), \quad (9)$$

in which  $\delta_L$  denotes the linear density field.  $b(k)$  is the bias and  $n(k)$  is defined such that the correlation  $\langle \delta_L(k)n(k) \rangle$  is zero. If we correlate  $\delta$  and  $\delta_L$ ,

$$\langle \delta(k)\delta_L(k) \rangle = b(k)\langle \delta_L(k)\delta_L(k) \rangle, \quad (10)$$

we can solve for  $b$  as

$$b(k) = \frac{P_{\delta\delta_L}(k)}{P_{\delta_L}(k)}. \quad (11)$$

Non-linear evolution drives  $b(k)$  to drop from unity, and generates the nonlinear term  $n(k)$ . Correlating  $\delta$  and itself,

$$\langle \delta(k)\delta(k) \rangle = b^2(k)\langle \delta_L(k)\delta_L(k) \rangle + \langle n(k)n(k) \rangle, \quad (12)$$

we find

$$P_\delta(k) = \mathcal{D}(k)P_{\delta_L}(k) + P_n(k), \quad (13)$$

where  $\mathcal{D}(k) \equiv b^2(k)$  is the nonlinear damping factor, and  $P_n$  is the mode coupling term.

With the help of Eq.11 and Eq.13, we can replace the partial derivatives  $\partial \ln P(k)/\partial \ln A$  in Eq.8 with

$$\frac{A}{P(k)} \frac{\partial P(k)}{\partial A} = \frac{P_{\delta\delta_L}^2(k)}{P_\delta(k)P_{\delta_L}(k)}, \quad (14)$$

which is just the square of the cross correlation function  $r^2(k)$ , of  $\delta$  and  $\delta_L$ .

The second partial derivative terms in Eq.8, the Hessian of the vector  $\ln P(k)$ , has the expectation value of the Fisher matrix with respect to the log powers. For linear density fields, the Fisher matrix is approximately equal to the inverse of the covariance matrix of power spectrum estimates, which should be diagonal, with diagonal elements equal to number of modes in each wavenumber bin (when considering  $\mathbf{k}$  and  $-\mathbf{k}$  as the same mode). Thus we can write down a simpler matrix product form of cumulative Fisher information,

$$I_A(< k_n) = r^2(k)^T [C_{\text{norm}}^{-1}(k, k')] r^2(k'), \quad (15)$$

where  $C_{\text{norm}}$  is the normalized covariance matrix with size per dimension up to  $k_n$ , defined as

$$C_{\text{norm}}(k, k') = \frac{\text{Cov}(k, k')}{\langle P(k) \rangle \langle P(k') \rangle}, \quad (16)$$

and  $r$  is the mean cross correlation of a given density field with linear one as a function of  $k$  up to  $k_n$ . It's reliable to define Eq.15 for nonlinear density fields as well, since the Fisher matrix is approximately the same as that of linear density fields on linear scales. The covariance matrix is defined as

$$\text{Cov}(k, k') \equiv \frac{\sum_{i,j=1}^N [P_i(k) - \langle P(k) \rangle] [P_j(k') - \langle P(k') \rangle]}{N-1}, \quad (17)$$

where angle brackets mean the expected values, and  $N$  is the total number of simulations. The cross-correlation



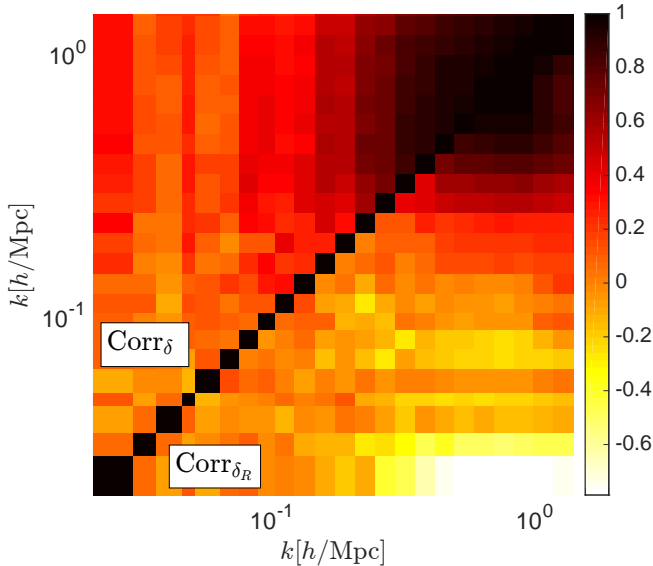


FIG. 3: Correlation coefficient matrix as found from 136 nonlinear power spectra (the upper-left elements) and the reconstructed power spectra (the lower-right off-diagonal elements). Both the matrix are symmetric and have unity diagonal elements.

coefficient matrix, or for short the correlation matrix, is the normalized version of the covariance matrix,

$$\text{Corr}(k, k') = \frac{\text{Cov}(k, k')}{\sqrt{\text{Cov}(k, k) \text{Cov}(k', k')}}, \quad (18)$$

which represents the correlation between different  $k$  modes. The correlation matrices for nonlinear and reconstructed power spectra are shown in Fig.3. For the nonlinear power spectra, the correlation matrix in the linear regime,  $k \lesssim 0.07 h/\text{Mpc}$ , is almost diagonal. The off-diagonal elements are produced by strong mode coupling in nonlinear scale, and the super-survey tidal effect which is small on linear scales but dominates in the weakly nonlinear regime [16]. The correlation matrix for the nonlinear power spectra has few negative elements ( $\text{Corr} \gtrsim -0.1$ ), which are produced by the unbiased error and thus will vanish with more simulations [17]. For the reconstructed correlation matrix, however, the linear regime expands up to  $k \simeq 0.3 h/\text{Mpc}$ , but number and magnitude of negative off-diagonal elements increases ( $\text{Corr} \gtrsim -0.8$ ).

Cumulative Fisher information is proportional to the volume. We plot the cumulative Fisher information per volume of the nonlinear, linear and reconstructed power spectra in Fig.4(a). The Fisher information of the nonlinear power spectra drops from the linear one at  $k \simeq 0.05 h/\text{Mpc}$ , and has a flat plateau in the translinear regime,  $k \simeq 0.3 h/\text{Mpc}$ , with a saturated value of  $I \simeq 2.5 \times 10^{-5}/(\text{Mpc}^3/h^3)$ . It indicates that there is nearly no independent information of the power spectrum in the translinear regime. But the information curve of the reconstructed power spectra keeps increasing roughly the same as the linear information until  $k \simeq 0.3 h/\text{Mpc}$ , and reaches its plateau at  $k \simeq 0.8 h/\text{Mpc}$

with the value of  $I \simeq 10^{-3}/(\text{Mpc}^3/h^3)$ , up by a factor of 40. It indicates that the MM reconstructed method can strongly recover the lost information within this scale. We compare the Fisher information given by the MM reconstruction method with the logarithmic density mapping method [3] as an example to illustrate its strength. We find that the MM reconstruction gives more than 10 times more information than logarithmic mapping. In some papers, the cross correlation  $r^2$  terms are set to be unity in Eq.15, which apparently increases the nonlinear information. We also plot those in Fig.4(b) for better comparison. We find that, in this case, the nonlinear information drops from the linear one beginning at the same scale,  $k \simeq 0.3 h/\text{Mpc}$ , but reaches the saturated value,  $I \simeq 4 \times 10^{-5}/(\text{Mpc}^3/h^3)$ , at translinear scale,  $k \simeq 0.2 - 0.8 h/\text{Mpc}$ . However, the MM reconstructed and logarithmic mapping information is higher than the linear one in the scale  $k \simeq 0.2 - 0.5 h/\text{Mpc}$ , which is not expected.

## V. DISCUSSION AND CONCLUSION

The new reconstruction method successfully recovers the lost linear information on the mildly nonlinear scale, increasing the saturated information from  $I \simeq 2.5 \times 10^{-5}/(\text{Mpc}^3/h^3)$  to at least  $I \simeq 10^{-3}/(\text{Mpc}^3/h^3)$ , and pushing the nonlinear scale to higher  $k$ . The result is better than previous methods (e.g. [3–5, 18]), and we believe that the reconstructed Fisher information will further increase to a greater magnitude in smaller scale since the cross correlation of the reconstructed power spectrum with the linear one increases in a higher resolution analysis [12]. The result in dark matter density fields gives a strong motivation to adapt the MM reconstruction to halo fields, neutrino fields, etc, so that we have access to the physics in smaller scales.

Reconstruction technique are concerned to improve cosmology measurements of BAO scale (e.g. [19, 20]). The successful application of the MM reconstruction on BAO reconstruction in 1D [8] and 3D [12] cosmology provide an intuitive view of the algorithm to push forward BAO research.

The MM reconstruction effectively decomposes the irrotational part and the curl part of the displacement field of particles. However, the reconstructed displacement might be greatly different from the real displacement in N-body simulation, since it is sensitive to the late stage shell-crossing and nonlinear process so that the original position of some specific particles are replaced by each other. It is meaningful to compare the irrotational displacement field through the MM reconstruction and through  $E$ -mode displacement reconstruction [9]. Since the MM reconstruction only needs the density field input and gives a large amount of recovering of lost information, it's expected to have a good effect on reconstructing the matter density field from observation.

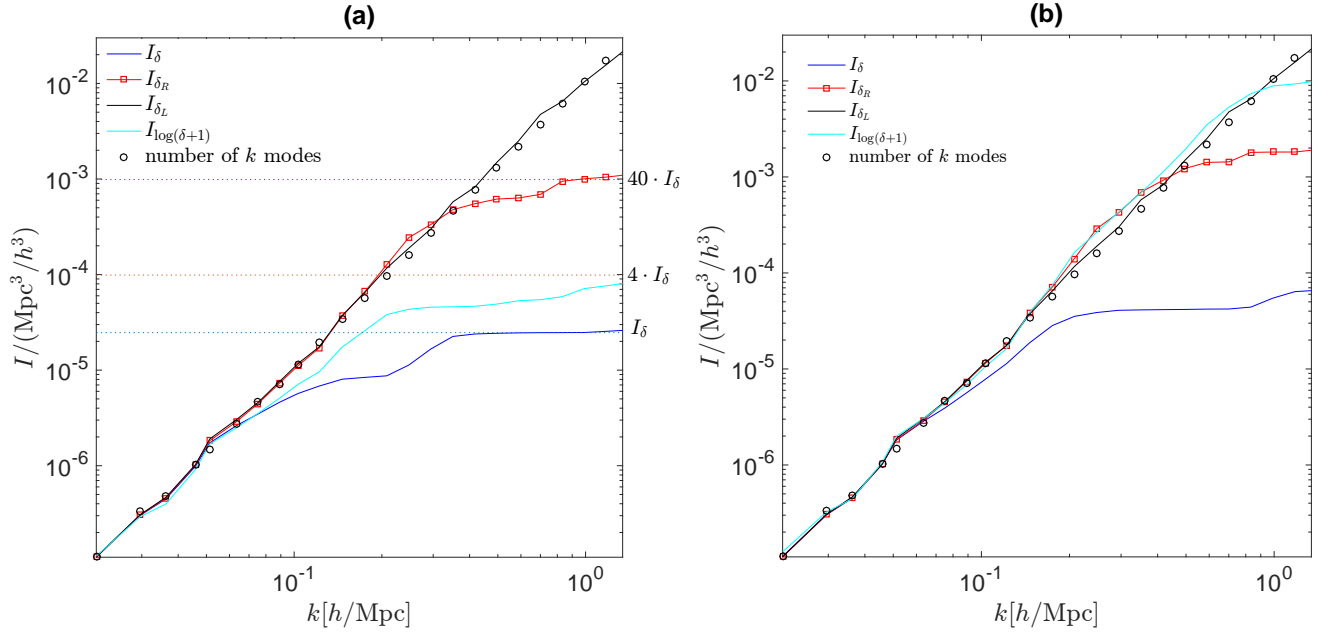


FIG. 4: (a) Cumulative Fisher information per volume in the power spectra as a function of wavenumber. The blue line corresponds to the nonlinear density fields; the red line with squares corresponds to the reconstructed density fields; the dark line corresponds to the linear density fields; the circles correspond to number of  $k$  modes up to that wave bin. Dotted lines correspond to saturated value of nonlinear Fisher information, 4 times and 40 times of it, respectively. (b) Cumulative Fisher information per volume given by setting the cross correlation to be unity. The black, blue and cyan lines match the results in [1, 3].

### Acknowledgments

We thank Hong-Ming Zhu, Yu Yu and Xin Wang for friendly and helpful discussions. Computations are performed on the General Purpose Cluster supercomputer

at the SciNet HPC Consortium. SciNet is funded by: the Canadian Foundation for Innovation under the auspices of Compute Canada; the Government of Ontario; Ontario Research Fund - Research Excellence; and the University of Toronto.

- 
- [1] C. D. Rimes and A. J. S. Hamilton, MNRAS **360**, L82 (2005), astro-ph/0502081.
  - [2] D. H. Weinberg, MNRAS **254**, 315 (1992).
  - [3] M. C. Neyrinck, I. Szapudi, and A. S. Szalay, ApJ **698**, L90 (2009), 0903.4693.
  - [4] T.-J. Zhang, H.-R. Yu, J. Harnois-Déraps, I. MacDonald, and U.-L. Pen, ApJ **728**, 35 (2011), 1008.3506.
  - [5] H.-R. Yu, J. Harnois-Déraps, T.-J. Zhang, and U.-L. Pen, MNRAS **421**, 832 (2012), 1012.0444.
  - [6] J. Harnois-Déraps, H.-R. Yu, T.-J. Zhang, and U.-L. Pen, MNRAS **436**, 759 (2013), 1205.4989.
  - [7] Y. B. Zel'dovich, A&A **5**, 84 (1970).
  - [8] H.-M. Zhu, U.-L. Pen, and X. Chen, ArXiv e-prints (2016), 1609.07041.
  - [9] H.-R. Yu, U.-L. Pen, and H.-M. Zhu, ArXiv e-prints (2016), 1610.07112.
  - [10] U.-L. Pen, ApJS **100**, 269 (1995).
  - [11] U.-L. Pen, ApJS **115**, 19 (1998), astro-ph/9704258.
  - [12] H.-M. Zhu, Y. Yu, U.-L. Pen, X. Chen, and H.-R. Yu (2016), 1611.09638.
  - [13] J. Harnois-Déraps, U.-L. Pen, I. T. Iliev, H. Merz, J. D. Emberson, and V. Desjacques, MNRAS **436**, 540 (2013), 1208.5098.
  - [14] A. Lewis, A. Challinor, and A. Lasenby, ApJ **538**, 473 (2000), astro-ph/9911177.
  - [15] M. Tegmark, A. N. Taylor, and A. F. Heavens, ApJ **480**, 22 (1997), astro-ph/9603021.
  - [16] K. Akitsu, M. Takada, and Y. Li, ArXiv e-prints (2016), 1611.04723.
  - [17] R. Takahashi, N. Yoshida, M. Takada, T. Matsubara, N. Sugiyama, I. Kayo, A. J. Nishizawa, T. Nishimichi, S. Saito, and A. Taruya, ApJ **700**, 479 (2009), 0902.0371.
  - [18] M. C. Neyrinck, I. Szapudi, and C. D. Rimes, MNRAS **370**, L66 (2006), astro-ph/0604282.
  - [19] D. J. Eisenstein, H.-J. Seo, E. Sirko, and D. N. Spergel, ApJ **664**, 675 (2007), astro-ph/0604362.
  - [20] M. White, MNRAS **450**, 3822 (2015), 1504.03677.
-